Theoretical Studies on the Mechanism of the Methane → Methanol Conversion Reaction Catalyzed by Methane Monooxygenase: O-Side vs N-Side Mechanisms

Harold Basch,*,†,‡ Djamaladdin G. Musaev,*,† Koichi Mogi,† and Keiji Morokuma*,†

Cherry L. Emerson Center for Scientific Computation and Department of Chemistry, Emory University, Atlanta, Georgia 30322, and Department of Chemistry, Bar Ilan University, Ramat Gan 52900, Israel

Received: October 31, 2000; In Final Form: January 9, 2001

The hybrid density functional method B3LYP was used to study the mechanism of the methane hydroxylation reaction catalyzed by the methane monooxygenase (MMO) enzyme. The key reactive compound **Q** of MMO was modeled by *cis*-$(H_2O)(NH_2)Fe(\mu\text{-}O)_2(\eta^2\text{-}HCOO)_2$ $Fe(NH_2)(H_2O)$, **I**, where the substrate molecule may coordinate to the bridging oxygen atoms, O^1 and O^2, located on the H_2O and NH_2 sides, leading to two different mechanisms, O-side and N-side pathways, respectively. Previously we have detailed the N-side pathway (Basch, H.; Mogi, K.; Musaev, D. G.; Morokuma, K. *J. Am. Chem. Soc.* **1999**, *121*, 7249); here we discuss the O-side pathway, and compare the two. Calculations show that, like the N-side pathway, the O-side pathway of the reaction of **I** with CH_4 proceeds via a *bound-radical mechanism*. It starts from the bis(μ-oxo) compound **I** and goes over the rate-determining transition state **III_O** for H abstraction from methane to form a weak complex **IV_O** between the Fe(μ-O)(μ-OH)Fe moiety and a methyl radical. This bound-radical intermediate **IV_O** converts to the oxo−methanol complex **VI_O** via a low barrier at transition state **V_O** for the addition of the methyl radical to the μ-OH ligand. Complex **VI_O** easily (with about 7−8 kcal/mol barrier) eliminates the methanol molecule and produces the Fe(μ-O)Fe, **VII_O**, complex. During the entire process, the oxidation state of the Fe core changes from Fe^{IV}−Fe^{IV} in **I** to a mixed-valence Fe^{III}−Fe^{IV} in the short-lived intermediate **IV_O**, and finally to Fe^{III}−Fe^{III} in **VI_O** and **VII_O**. A comparison of the O-side and N-side pathways shows that both include similar intermediates, transition states, and products. The rate-determining step of both pathways is the H-atom abstraction from the methane molecule, which occurs by 23.2 and 19.5 kcal/mol barrier for the O-side and N-side pathways, respectively, in the ground ^{9}A states of the systems. Thus, the N-side pathway is intrinsically more favorable kinetically than the O-side pathway by about 4 kcal/mol. However, experimentally in the enzyme the N side is blocked by unfavorable steric hindrance and the actual reaction has to take place on the O side.

I. Introduction

Methane monooxygenase (MMO) is an enzyme that catalyzes the conversion of the inert methane molecule to methanol.[1−3] During this reaction the O−O bond of O_2 is cleaved, followed by reduction of one of the O atoms to water, and incorporation of the second one into the substrate to yield methanol:

$$CH_4 + O_2 + NAD(P)H + H^+ \rightarrow CH_3OH + NAD(P)^+ + H_2O \quad (1)$$

The best-characterized forms of the soluble MMO (sMMO) contain[2,4] three protein components: hydroxylase (MMOH), the so-called B component (MMOB), and reductase (MMOR), each of which is required for efficient substrate hydroxylation coupled to NADH oxidation. The hydroxylase, MMOH, which binds O_2 and substrate and catalyzes oxidation, is a dimer, each half of which contains three types of subunits (α, β, γ) and a hydroxy-bridged binuclear iron cluster in the α subunit. In the resting state of MMOH ($MMOH_{ox}$), the diiron cluster is in the diferric state [Fe^{III}−Fe^{III}], which can accept one or two electrons to generate the mixed-valence [Fe^{III}−Fe^{II}] or diferrous state [Fe^{II}−Fe^{II}], respectively.

X-ray crystallographic studies of the enzyme from *Methylococcus capsulatus* (Bath)[5] and *Methylosinus trichosporium* OB3b[6] have demonstrated that in $MMOH_{ox}$ each Fe center has a six-coordinate octahedral environment (see Chart 1). The Fe ions are bridged by a hydroxide ion, a bidentate Glu γ-carboxylate, and a water or hydroxyl molecule (or another carboxylate). In addition, each Fe ion is coordinated by one His nitrogen ligand and one monodentate Glu carboxylate. The two Fe centers are different from each other in that one of them (Fe^2) has an additional monodentate glutamate carboxylate, while the other Fe (Fe^1) has one additional water molecule. Upon reduction, one of the carboxylate ligands undergoes a so-called "1,2-carboxylate shift" from being a terminal, monodentate ligand bound to Fe^2 to being a monodentate, bridging ligand between the two irons, with the second oxygen of this carboxylate also weakly coordinated to Fe^2. In addition, the hydroxy bridge is lost, and the other hydroxy/water bridge shifts from serving as a bridge to being terminally bound to Fe^1. Also, the terminal water bound to Fe^1 in the oxidized form of MMOH seems to move out of the first coordination sphere upon reduction of the cluster. Thus, in the reduced form of $MMOH_{red}$ the ligand environment of the Fe ions becomes effectively five-coordinated, which is reasonable since this is the form of the cluster that coordinates and activates dioxygen.

The latest experimental[7] and theoretical[8] studies have confirmed the above-mentioned high flexibility of the ligand

† Emory University.
‡ Bar Ilan University.

10.1021/jp004032k CCC: $20.00
Published on Web 03/13/2001

CHART 1: Structural Representation of the Binuclear Fe Center of Diferric $MMOH_{ox}$ and Diferrous $MMOH_{red}$[a]

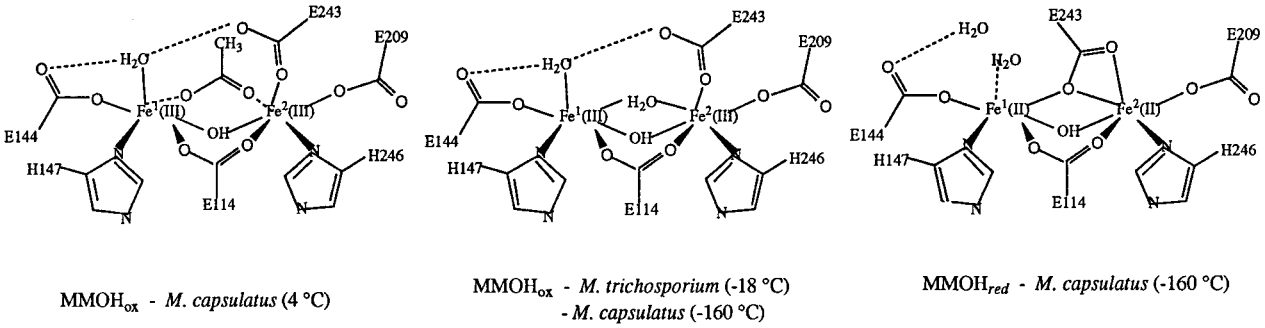

$MMOH_{ox}$ - *M. capsulatus* (4 °C)

$MMOH_{ox}$ - *M. trichosporium* (-18 °C)
- *M. capsulatus* (-160 °C)

$MMOH_{red}$ - *M. capsulatus* (-160 °C)

[a] After ref 2a.

SCHEME 1: Experimentally Proposed Catalytic Cycle of MMO[a]

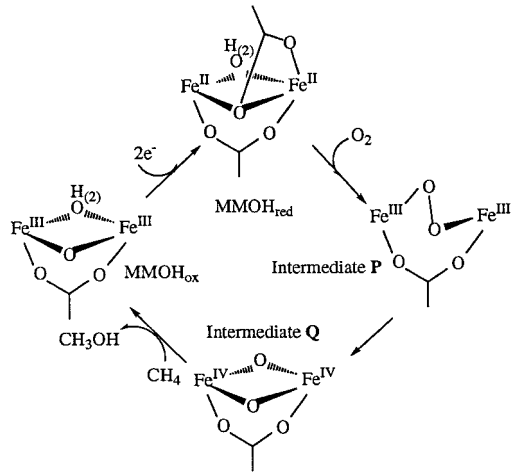

[a] See ref 2a.

environment of Fe centers of MMOH. These studies show that the 1,2-carboxylate shift, as well as monodentate ↔ bidentate rearrangement of a terminal carboxylate ligand, takes place very easily in the MMOH. Moreover, these reactions can take place *reversibly*, under the proper experimental conditions. In the literature[7a,8] this ligand flexibility has been postulated to be one of the important factors for the proper functioning of the enzyme. Indeed, the flexibility of the carboxylate type of ligands (such as glutamates and aspartates) allows them to coordinate to the Fe centers depending on enzymatic needs, as bidentate ligands (bridging or chelating) when saturation of the first coordination sphere of Fe centers is required, and as monodentate (terminal) ligands when one or more vacant coordination sites in the Fe centers are needed (for example, upon dioxygen or substrate coordination) to enable a certain reaction step to take place.

It has been established[2a,3] that the diferrous state of hydroxylase ($MMOH_{red}$) is the only one capable of reacting with dioxygen and initiating the catalytic cycle. It reacts very fast with O_2 and forms a metastable compound **O**, which spontaneously converts to compound **P** (see Scheme 1). Spectroscopic studies[9] indicate that compound **P** is a peroxide species, where both oxygens are bound symmetrically to the irons. Compound **P** spontaneously transforms to compound **Q**, which was proposed to contain two antiferromagnetically coupled high-spin Fe^{IV} centers. EXAFS and spectroscopic studies[2b,10] of compound **Q**, which was trapped from *M. trichosporium* OB3b and *M. capsulatus*, have demonstrated that compound **Q** has a diamond core $(Fe^{IV})_2(\mu\text{-}O)_2$ structure with one short (1.77 Å) and one long (2.05 Å) Fe−O bond per Fe atom and a short Fe−Fe distance of 2.46 Å. Compound **Q** has been proposed to be the key oxidizing species for MMO.

In the literature several mechanisms[2a,11] for the reaction of (a) $MMOH_{red}$ with molecule O_2 and (b) intermediate **Q** with alkane have been proposed. Despite these efforts, the mechanisms of these catalytic reactions still remain unclear and need additional and comprehensive study using different techniques. Since the mechanism of the reaction of $MMOH_{red}$ with the O_2 molecule and our latest contributions[12] to that will be discussed separately, here we continue[13] our discussions on the mechanism of the reaction of intermediate **Q** with a molecule of methane.

Thus, the purpose of our series of papers is to study the mechanism of the reaction

$$\{Fe_2(\mu\text{-}O)_2\}_{\mathbf{Q}} + CH_4 \rightarrow \{Fe_2(\mu\text{-}O)(\mu\text{-}HOCH_3)\} \rightarrow \{Fe_2(\mu\text{-}O)\} + HOCH_3 \quad (2)$$

In general, the experimentally proposed mechanisms for the reaction of intermediate **Q** with alkane can be divided into two different classes: (1) radical and (2) nonradical mechanisms. The radical mechanism starts with abstraction of the hydrogen atom from the substrate to form **QH** (hydroxyl-bridged **Q** compound) and free alkyl radical, while the nonradical mechanism implies a concerted pathway, occurring via a four-center transition state and leading to a "hydrido−alkyl−**Q**" compound. The latest experimental studies[14] show that the mechanism of this reaction is more complex, and could even be different for the enzyme isolated from different organisms; radical clock substrate probe studies with sMMO isolated from *M. capsulatus* (Bath) afforded no evidence for formation of a substrate radical, while, for the enzyme isolated from *M. trichosporium* OB3b, evidence for a substrate radical was detected. Thus, the elucidation of the true mechanism of this process and the factors affecting it are still open questions and require further studies. To provide some insight into these nontrivial questions, we have here performed quantum chemical calculations of the structure (both geometrical and electronic) and energetics of intermediates and transition states of the reaction of intermediate **Q** with a molecule of methane. However, to conduct quantum chemical research, one at first has to answer several nontrivial questions.

First, one has to choose a reasonable model for the intermediate **Q** incorporating all available experimental findings. According to our previous studies,[8,12,13] the smallest reasonable model of compound **Q** satisfying all experimental conditions is *cis*-$(H_2O)(NH_2)Fe(\mu\text{-}O)_2(\eta^2\text{-}HCOO)_2Fe(NH_2)(H_2O)$, **I** (see Figure 1), which was also chosen to be our working model throughout this paper.

The second important question is the spin state of the system. Spectroscopic studies[2,3] show that compound **Q** is diamagnetic, suggesting that compound **Q** contains two antiferromagnetically

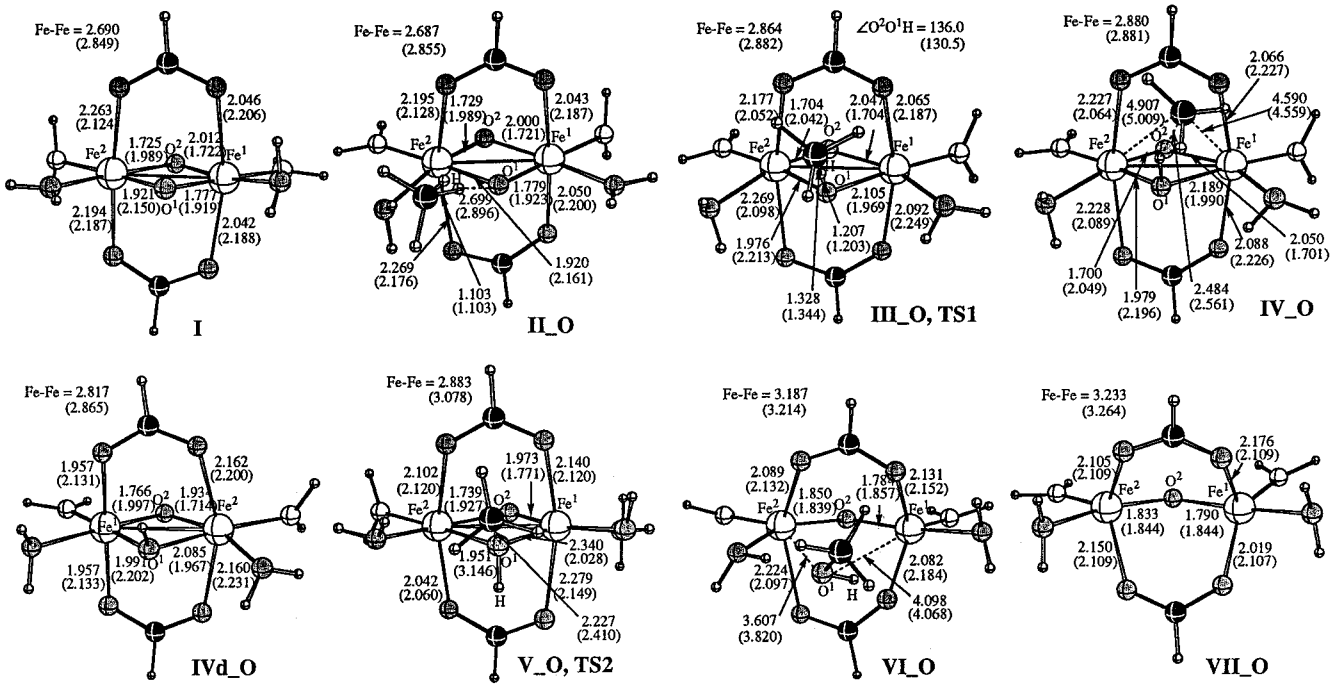

Figure 1. Calculated structures (distances in angstroms, angles in degrees) of the intermediates and transition states of the O-side pathway of the reaction $(NH_2)(H_2O)Fe(\mu\text{-}O)_2(\eta^2\text{-}HCOO)_2Fe(NH_2)(H_2O) + CH_4 \rightarrow (NH_2)(H_2O)Fe(\mu\text{-}O)(\mu\text{-}HOCH_3)(\eta^2\text{-}HCOO)_2Fe(NH_2)(H_2O)$. Numbers for the ^{9}A state are without parentheses, and those for the ^{11}A state are in parentheses.

coupled high-spin Fe^{IV} atoms. The complex is EPR silent, and the exchange coupling J constant is found to be relatively large, >60 cm^{-1}. This is also consistent with the short, 2.46 Å, Fe−Fe distance of compound **Q**.

The third problem is the choice of adequate computational methods and approximations. Here, the problem comes from the representation of the open-shell low-spin coupling ($2S + 1 = 0$) of the two paramagnetic centers by a single-determinant method (such as DFT); the "restricted" calculations for the low-spin state give the closed-shell singlet state, which cannot represent open-shell atoms. An "unrestricted" calculation with a low M_S value gives a heavily spin-contaminated state or a symmetry-broken wave function, which do not represent a true eigenstate. Here, one should use a multireference method (such as MCSCF, CASPT2, etc.), which, unfortunately, is impractical for such large systems. Therefore, when the magnitude of the spin coupling between the two centers is not strong, it is more practical to ignore the antiferromagnetic nature of these systems, and to perform spin-unrestricted open-shell single-determinant calculations for ferromagnetically coupled high spin states. This type of approach also retains the proper spins on individual metal (Fe) atoms. Since the magnitude of the spin coupling between the two centers of **Q** is relatively small, as discussed above, we expect that the mechanism of the reaction studied below is not much influenced by the antiferromagnetic nature of the complexes.

As seen in Figure 1, in general, the substrate methane molecule may coordinate and react with the bridging oxygen atoms O^1 and O^2 located on the H_2O and NH_2 sides, respectively, of structure **I**. These two pathways are called below O-side and N-side pathways, respectively. According to experimental data,[2,3] the only valid pathway is by coordination of the substrate from the O side, because of the existence of the substrate coordination pocket; the coordination of substrate from the N side is sterically hindered and not available. Despite that, in our previous paper,[13] we found that the N-side pathway is intrinsically very reactive. In the present paper, we discuss the O-side pathway and compare the intrinsic reactivities of the two sides.

Previously, several theoretical attempts[15−17] have been made to model MMOH and to study the mechanism of the hydroxylation reaction. However, these early studies used either unrealistic or small models, such as FeO^+,[15] $Fe_2(OH)_3(H_2O)_2(HCOO)(\mu\text{-}O)_2$,[16a] $Fe_2(OH)_4(H_2O)_4(\mu\text{-}O)_2$,[16a] and $(H_2O)_2Fe(\mu\text{-}O)_2Fe(H_2O)$,[16a,b] or low-level theoretical models such as the extended Hückel method. While later more realistic models were proposed and used,[16c,17] these studies, however, concentrated either on O_2 coordination and the O−O bond activation processes or on the structures and stabilities of the $MMOH_{red}$ and $MMOH_{ox}$.

This paper is organized as follows: In section II we briefly discuss the computational procedures used here, section III includes the main conclusions from our previous paper on the studies of the N-side mechanism of reaction 2, in section IV we discuss our results on the O-side mechanism, section V briefly compares N-side and O-side mechanisms, and, finally, in section VI we draw a few conclusions from these studies.

II. Computational Procedure

As mentioned above, on basis of available experimental data[2,3] and our previous studies,[8,12,13] we use our smallest reasonable model of compound **Q,** *cis*-$(H_2O)(NH_2)Fe(\mu\text{-}O)_2(\eta^2\text{-}HCOO)_2Fe(NH_2)(H_2O)$, **I** (see Figure 1), throughout this paper. Since the magnitude of the antiferromagnetic spin coupling between the two Fe centers of the diamagnetic compound **Q** is not strong (see above discussion), we expect that the mechanism of reaction 2 is not much influenced by the antiferromagnetic nature of the complex. Therefore, we performed spin-unrestricted open-shell single-determinant calculations for ferromagnetically coupled high-spin states with multiplicities of $2M_S + 1 = 9$ and 11, ^{9}A and ^{11}A, respectively. In these calculations we used the hybrid density functional method, B3LYP,[18] in conjunction

with the Stevens−Basch−Krauss (SBK) effective core potentials (ECPs) and the standard split-valence 31G, CEP-31, and (8s8p6d/4s4p3d) basis sets for H, (C, O, and N), and Fe atoms, respectively,[19] which we call the SBK basis set and which is used for geometry optimization. The energies were recalculated at the B3LYP/SBK optimized geometries with two polarization basis sets at the B3LYP level. SBK(O*) is the SBK basis set augmented by a polarization d function ($\alpha = 0.85$) on all the oxygen atoms except those on two terminal water molecules. The largest basis set SBK(CO*) adds to SBK(O*) a polarization d function ($\alpha = 0.75$) on the carbon atom of methane. Previously, the B3LYP method with a double-ζ-quality basis set has been shown to be quite reliable in both the geometry and energy of transition-metal complexes.[20]

All calculations were performed using the Gaussian-94 package.[21] Since the systems studied here were too large for our computer resources, second-derivative calculations were not performed. To confirm the nature of the calculated TS, quasi-IRC (intrinsic reaction coordinate) calculations were carried out in the following manner. The geometry of the transition state was at first shifted, toward both the reactant and the product sides, on the basis of the eigenvector of the imaginary frequency of the approximate Hessian, and then was released for equilibrium optimization. In this manner, each transition state was "connected" to the reactant and the product of the respective step.

The energies given here and discussed below do not include zero-point energy correction (ZPC) or any other spectroscopic or thermodynamic terms. Note that below we will discuss only the energetics calculated at our best B3LYP/SBK(CO*) level using B3LYP/SBK optimized geometries. As one can see from Table S1 in the Supporting Information, SBK and SBK(O*) basis sets provide qualitatively the same results as those with SBK(CO*). However, the calculated relative energies can differ up to 8 kcal/mol. The main differences appear in the methanol dissociation energies, especially for the ^{11}A state. The general tendency is that an improved basis set increases the methane C−H bond activation barrier relative to the methane complex, and increases the exothermicity of the methanol formation reaction.

III. Summary of Our Previous Studies on the N-Side Pathway Mechanism

From our previous studies[13] on the N-side pathway of reaction 2, one can draw the following conclusions.

(1) The qualitative features of potential energy profiles of the reaction of compound **Q** with CH_4 are qualitatively similar between the ^{9}A and ^{11}A states. In both states, the reaction starts from the bis(μ-oxo) compound **I** (model of **Q**) and goes over the rate-determining transition state **III_N** corresponding to H-atom abstraction (by the O^2 atom) from CH_4 to the form a bound-radical intermediate **IV_N** in which the (μ-O^1)(μ-O^2H) moiety is complexed weakly with the methyl radical. This intermediate **IV_N** is presumably short-lived and is not likely to be easily detected experimentally, as it is connected via a low barrier at transition state **V_N** to the addition of the methyl radical to the μ-OH ligand to produce the oxo−methanol complex **VI_N**. The entire reaction proceeds via *a bound-radical mechanism*, with the barrier for the rate-determining step, methane H-abstraction, of 19 kcal/mol and an overall exothermicity of 39 kcal/mol.

(2) At reactant **I**, the ^{9}A state is lower than the ^{11}A state by 8.8 kcal/mol, which is reduced to 3.7 kcal/mol at TS1 **III_N** corresponding to the hydrogen abstraction step. The ^{9}A state of **I** has, qualitatively speaking, an Fe^{IV}−Fe^{IV} core, as suggested experimentally for **Q**, while the ^{11}A state of **I** has an Fe^{IV}−Fe^{III} core and is less stable. Once the system reaches the bound-radical hydroxyl intermediate **IV_N**, calculations for both ^{9}A and ^{11}A converge to the same electronic state with the same structure and energy, corresponding to the Fe^{IV}−Fe^{III} mixed-valence state interacting weakly with the methyl radical either ferro- or antiferromagnetically. In the product methanol complex **VI_N**, the ^{11}A state is 8.4 kcal/mol lower than the ^{9}A state. Here, the preferred iron core is found to be Fe^{III}−Fe^{III} and each Fe has five spins, which naturally gives the ^{11}A state when ferromagnetically coupled.

(3) Therefore, the overall mechanism of reaction 2 is found to be

I, $L_4Fe^{IV}(\mu\text{-}O)_2Fe^{IV}L_4 + CH_4 \rightarrow$ **III_N**, TS1 for H-atom abstraction (rate-determining) → **IV_N**, $L_4Fe^{IV}(\mu\text{-}O^1)(\mu\text{-}O^2H(\cdots CH_3))Fe^{III}L_4$ (bound-radical intermediate) → **V_N**, TS2 for CH_3 addition → **VI_N**, $L_4Fe^{III}(O^2HCH_3)(\mu\text{-}O^1)Fe^{III}L_4$

During the reaction, the oxidation state of the Fe core changes from Fe^{IV}−Fe^{IV} in **I** to a mixed-valence Fe^{IV}−Fe^{III} in the short-lived intermediate **IV_N**, and finally to Fe^{III}−Fe^{III} in **VI_N**. Thus, although the methane activation takes place on one of the oxo oxygens, the iron atoms actively participate in the reaction and manipulate the spin recoupling and bond breaking/formation during the overall reaction 2.

IV. Results and Discussion for the O-Side Pathway

The important geometrical parameters of the reactants, intermediates, and transition states calculated at the B3LYP/SBK level are shown in Figure 1. Their full geometrical parameters are included in the Supporting Information. The energies of these structures calculated at the B3LYP level with basis set SBK(CO*) are presented in Table 1. Table 2 shows the calculated Mulliken spin densities of selected atoms and fragments for the optimized structures. In Figure 2 we present the potential energy profiles for the ^{9}A and ^{11}A states of the O-side pathway of the reaction of compound **Q** with a molecule of methane.

Reactant Complex, I. The calculated structural parameters and energetics of complex **I**, which is a model of compound **Q**, have been discussed earlier.[13] However, here we report new structures and energies for complex **I**. The total energies of the structures reported here are a few kilocalories per mole lower than those reported in our previous paper, and considered to be more accurate. In general, the conclusions drawn previously are fully valid for the new structures of complex **I** presented in Figure 1. First, calculations show that compound **I** can be formally written as $L_4Fe(\mu\text{-}O)_2FeL_4$, where the "diamond core" Fe_2O_2 has an asymmetric structure; one of the diamond core O atoms is located closer to one Fe center, and the second one is closer to the other Fe center. Second, the ground state of compound **I** is the ^{9}A state, an Fe^{IV}−Fe^{IV} complex, where a spin density of roughly seven out of the total of eight is localized on the two Fe atoms, with about 0.74e delocalized onto the bridging O atoms and the rest on the bridging carboxylates. However, the newly calculated ^{11}A state with an Fe^{IV}−Fe^{III} complex and 10 unpaired electrons is only 5.4 kcal/mol higher in energy vs 8.8 kcal/mol reported previously. As seen in Table 1, this difference between the current and previously calculated

TABLE 1: Total (in Italics, hartrees) and Relative (kcal/mol, Relative to the ^{9}A Reactants) Energies of Various Intermediates and Transition States, for ^{9}A and ^{11}A States, for the Reaction of Complex I with a Molecule of Methane, Calculated at the B3LYP/SBK(CO*) Level[a]

structure		O side	N side
		^{9}A State	
reactants	**I** + CH_4	0.0	0.0
		−419.775345	*−419.775082*
CH_4 complex	**II**	**−1.5**	−0.7
TS1 (C−H)	**III**	23.2	19.5
OH···CH_3 complex	**IV**	11.3	11.4
TS2 (O−CH_3)	**V**	20.6	18.2
CH_3OH complex	**VI**	−41.8	−31.4
CH_3OH dissoc	**VII**	−34.3	
CH_3 dissoc	**IVd**	23.7	13.5
		^{11}A State	
reactants	**I** + CH_4	5.4/0.0	8.8/0.0
		−419.766739	*−419.761076*
CH_4 complex	**II**	4.2/−1.2	8.5/−0.3
TS1 (C−H)	**III**	24.4/19.0	23.2/14.4
OH···CH_3 complex	**IV**	11.3/5.9	11.8/3.0
TS2 (O−CH_3)	**V**	18.6/13.2	17.6/8.8
CH_3OH complex	**VI**	−53.9/−59.3	−39.8/−48.6
CH_3OH dissoc	**VII**	−46.7/−52.1	
CH_3 dissoc	**IVd**	15.5/10.1	−13.4/4.6

[a] Corresponding energies calculated at the B3LYP/SBK and B3LYP/SBK(O*) levels for the O-side pathway are given in the Supporting Information, Table S1. The numbers after the slash are relative to the ^{11}A reactants.

TABLE 2: Mulliken Atomic Spin Densities (e) for the Various Intermediates and Transition States for the O-Side Pathway of Reaction 2 of MMO with Methane, Calculated at the B3LYP/SBK Level[a]

	atomic spin densities (e)					
structure	L_nFe^2	L_nFe^1	O^2	O^1	H[b]	CH_3[c]
		^{9}A State				
I	3.44	3.55	0.44	0.30		
II_O	3.43	3.52	0.44	0.31		
III_O	4.59	3.54	0.40	−0.37	0.06	−0.55
IV_O	4.64	3.51	0.43	0.08	0.00	−0.99
V_O	4.58	3.23	0.38	0.20	0.00	−0.73
VI_O	4.54	2.92	0.35	0.00	0.00	0.00
VII_O	4.49	2.95	0.38	0.00	0.00	0.00
IVd_O	4.52	1.69	0.56	0.07	0.00	0.99
		^{11}A State				
I	4.62	3.47	1.03	0.43		
II_O	4.62	3.47	1.03	0.43		
III_O	4.63	3.52	0.43	0.55	−0.07	0.59
IV_O	4.67	3.58	0.43	0.10	0.00	0.98
V_O	4.57	3.97	0.50	0.01	0.01	0.81
VI_O	4.48	4.59	0.66	0.00	0.00	0.00
VII_O	4.54	4.54	0.67	0.00	0.00	0.00
IVd_O	4.65	4.54	0.42	0.08	0.00	0.99

[a] Here, L_nFe stands for the $(H_2O)(NH_2)Fe$ fragment. This table does not include the portion of spin densities located on the bridging carboxylate ligands, each of which may have about 0.10−0.15e spin. [b] H atom located between O^2 and CH_3 fragments. [c] The number for the entire CH_3 fragment.

^{9}A−^{11}A energy gap is mainly due to stabilization of the ^{11}A state of **I**. Upon going from ^{9}A to ^{11}A, the spin densities on the Fe centers are increased by one and those on the bridging O centers are also increased by 0.72e, indicating that the ^{9}A → ^{11}A transition corresponds to moving one electron from a weakly Fe−O bonding orbital of the Fe_2O_2 core to its weakly antibonding (or nonbonding) partner. All these conclusions are consistent with the available experimental findings.[2]

Methane−Q Complex, II_O. The coordination of a methane molecule to the O^1 atom on the O side of compound **I** leads to the methane−**Q** complex, structure **II_O**. Since the interaction between methane and structure **I** is extremely weak, the geometries of the CH_4 and **I** fragments in complex **II_O** are very close to those in the free CH_4 and **I**, respectively. The complexation energy is calculated (relative to the corresponding reactants) to be 1.5 and 1.2 kcal/mol for the ^{9}A and ^{11}A states, respectively. Because of unfavorable zero-point energy and entropy factors, it is very likely that **II_O** does not exist in reality, and therefore, we will not discuss it in detail.

Transition State, III_O, and Product, IV_O, for C−H Activation. Our calculations show that the activation of the methane C−H bond takes place via transition state **III_O**. As seen from Figure 1, in the transition state **III_O** the C−H bond to be broken is elongated from 1.103 Å in **II_O** to 1.328 and 1.344 Å for the ^{9}A and ^{11}A states, respectively. Furthermore, the O−H bond is nearly formed at 1.207 and 1.203 Å at the TS. Comparison of the geometries of **III_O** for ^{9}A and ^{11}A states shows that they are very similar for the active parts. The geometrical parameters indicate clearly that **III_O** is a TS corresponding to the H-abstraction process for both (^{9}A and ^{11}A) states. The "quasi-IRC" calculations actually confirm that structure **III_O** is the transition state connecting **II_O** with the product **IV_O** for both ^{9}A and ^{11}A states. The H-abstraction barriers are calculated to be 24.7 and 20.2 kcal/mol for the ^{9}A and ^{11}A states, respectively, relative to the corresponding CH_4 complex **II_O**. These values of the barrier are in fairly good agreement with available experimental estimates, 14−18 kcal/mol.[14]

Overcoming this transition state leads to the product complex **IV_O**, which is an oxo/hydroxyl−methyl complex, formally written as $L_4Fe(\mu\text{-}O)(\mu\text{-}OH\cdots CH_3)FeL_4$, with the methyl radical weakly interacting via a OH···C interaction (see Figure 1). The Fe^1−O^2 bond elongates from 2.000 to 2.050 Å, while the Fe^2−O^2 bond is shortened from 1.729 to 1.700 Å upon going from **II_O** to **IV_O** for the ^{9}A state. The Fe^1−O^1H and Fe^2−O^1H bonds are 2.189 and 1.979 Å in structure **IV_O**, compared to the corresponding Fe−O distance of 1.779 and 1.920 Å in structure **II_O** for the ^{9}A state. The corresponding changes are less significant for the ^{11}A state.

The spin densities for structures **III_O** and **IV_O** are found to be similar to each other within their respective ^{9}A and ^{11}A states, except for those on the $O^1\cdots H\cdots CH_3$ fragment. The spin densities of this group for the ^{9}A and ^{11}A states are of the same magnitude but opposite sign. In TS **III_O** a radical center begins to develop on the CH_3 group, with spin densities of −0.55 and +0.59 for the ^{9}A and ^{11}A states, respectively. In intermediate **IV_O**, the CH_3 group is now a radical with spin densities of −0.99 and +0.98 for the ^{9}A and ^{11}A states, respectively. The formal oxidative states of Fe^1 and Fe^2 in **IV_O** can be considered to correspond to Fe^{IV} with four spins and Fe^{III} with five spins for both states. Thus, in going from **I** to **IV_O**, the oxidation state goes from Fe^{IV}−Fe^{IV} to Fe^{III}−Fe^{IV} for the ^{9}A state, while for the ^{11}A state the oxidation state remains to be Fe^{III}−Fe^{IV}. Since the two Fe centers are coupled ferromagnetically in both ^{9}A and ^{11}A states, the spin of the CH_3 radical in both **III_O** and **IV_O** has to couple antiferromagnetically (with negative spin) and ferromagnetically (with positive spin) to make the total spin $2S + 1$ equal to 9 and 11, respectively.

As seen in Table 1, the bound radical complex lies energetically 12.4 and 4.2 kcal/mol below the dissociation limit $L_4Fe(\mu\text{-}O)(\mu\text{-}OH)FeL_4$(structure **IVd_O**) + CH_3 for the ^{9}A and ^{11}A states, respectively. With consideration of the entropy effects, this CH_3 binding energy will be reduced roughly by about 10 kcal/mol, and the CH_3 binding free energy will be only a few

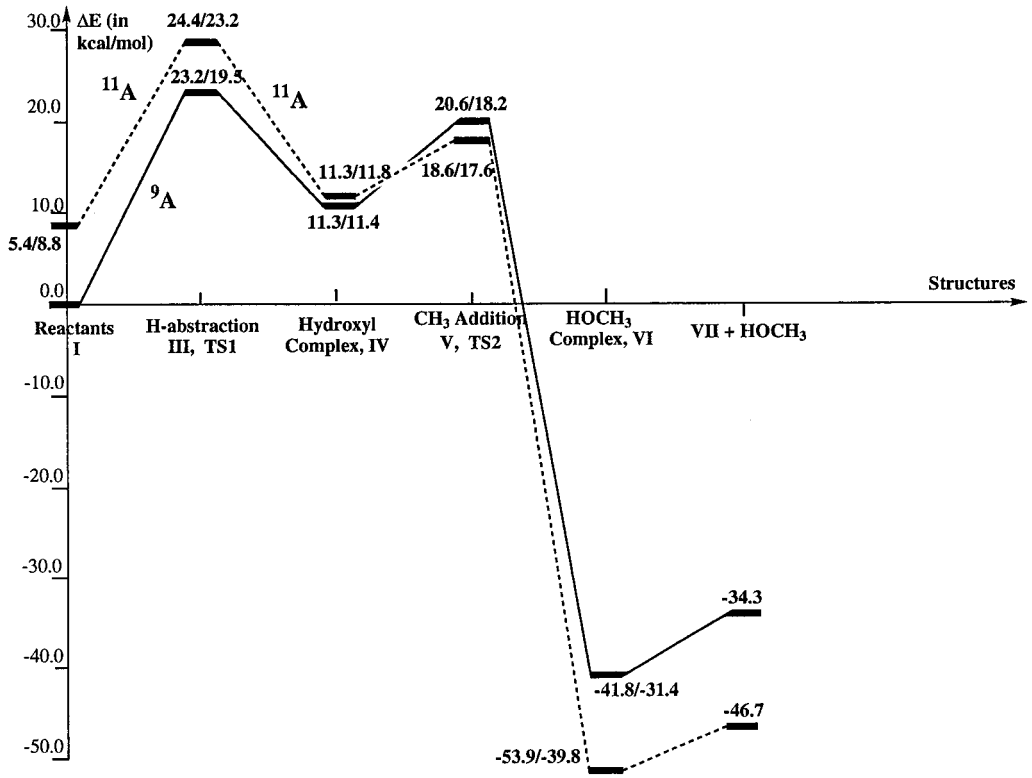

Figure 2. Potential energy profile (kcal/mol) at the B3LYP/SBK(CO*)// B3LYP/SBK level for both the ^{9}A state and the ^{11}A state of the methane activation reaction via O-side and N-side (after slash) pathways: $(NH_2)(H_2O)Fe(\mu\text{-}O)_2(\eta^2\text{-}HCOO)_2Fe(NH_2)(H_2O) + CH_4 \rightarrow (NH_2)(H_2O)Fe(\mu\text{-}O)(\mu\text{-}HOCH_3)(\eta^2\text{-}HCOO)_2Fe(NH_2)(H_2O)$.

kilocalories per mole, suggesting that a fraction of bound CH_3 radical can dissociate before conversion to the methanol complex takes place. The present analysis clearly demonstrates that the methane oxidation proceeds via a bound-radical mechanism, which is in good qualitative agreement with the radical clock probe experiments of Lippard et al.[22] on the oxidation of ethane and butane, where it was shown that only 71−78% of the reaction takes place with retention of configurations.

The entire process **I** + $CH_4 \rightarrow$ **IV_O** is calculated to be endothermic by 11.3 kcal/mol for both ^{9}A and ^{11}A states. The general conclusion from the above-presented results is that the O-side reaction of compound **Q** with a methane molecule occurs via a "bound-radical" mechanism. The same conclusion was drawn for the N-side pathway in our previous paper.[13]

Transition State, V_O, and Product, VI_O, for Methanol Formation. In the next step of the reaction, the C−O bond is formed between the carbon atom of the methyl radical and the O^1 atom of the O^1H bridge, which is found to occur via transition state **V_O**. As seen in Figure 1, this transition state is an early TS since the geometries of the "active part" are very close to those of intermediate **IV_O**: the O^1−CH_3 bond that is being formed is calculated to be 2.227 and 2.410 Å for the ^{9}A and ^{11}A states, respectively. As the methyl radical approaches from the top of the core $Fe^1O^1Fe^2O^2$ plane to the hydroxyl ligand O^1H, the H atom of the latter bends down, to create a tetrahedral tetracoordinate O^1 environment. Apparently this bend costs some energy. The barrier heights for the CH_3 addition to the hydroxyl ligand calculated relative to the intermediate **IV_O** are calculated to be 9.3 and 7.3 kcal/mol for the ^{9}A and ^{11}A states, respectively. Obviously, this step of the reaction is not rate-determining, and can occur rather fast.

Overcoming the barrier at **V_O** leads to the methanol complex **VI_O**. As seen in Figure 1, upon reaction of the methyl group with the diamond HO^1 group, the Fe^1−O^1 and Fe^2−O^1 bonds are elongated significantly for both states; they are calculated to be 3.607 and 4.098 Å for the ^{9}A state, and 3.820 and 4.068 Å for the ^{11}A state. In other words, structure **VI_O** can be formally written as a weakly bound methanol complex of $L_4Fe(\mu\text{-}O^2)FeL_4$. The overall reaction **I** + $CH_4 \rightarrow$ **VI_O** is calculated to be exothermic by 41.8 and 53.9 kcal/mol for the ^{9}A and ^{11}A states, respectively. The calculated methanol complexation energy with the $L_4Fe(\mu\text{-}O^2)FeL_4$ fragment, structure **VII_O**, is 7.5 and 7.2 kcal/mol for the ^{9}A and ^{11}A states, respectively. This is consistent with the above-presented geometries of complex **VI_O**, as well as complex **VII_O**; dissociation of the methanol molecule, HO^1CH_3, from **VI_O** does not change geometries. Indeed, as seen in Figure 1, the important geometric parameters of **VI_O** and **VII_O** are very close. Table 2 shows that, in the ^{11}A state, upon going from the hydroxyl complex **IV_O** to the methanol complex **VI_O**, Fe^1 changes its formal oxidation state from Fe^{IV} with four spins to Fe^{III} with five spins, while the spin density on the methyl radical is completely annihilated upon forming a covalent bond between CH_3 and O^1H. The transition state **V_O** has a spin distribution between those of **IV_O** and **VI_O** for both electronic states. On the other hand, in the ^{9}A state, upon going from the hydroxyl complex **IV_O** to the methanol complex **VI_O**, the spin density on Fe^1 is reduced by about 0.6, corresponding to the disappearance of roughly one unpaired electron. Since Fe^V is not a stable species, it is most likely Fe^1 changed its formal oxidation state from Fe^{IV} with four spins to Fe^{III} with five formal d electrons. Because of the restriction $2S + 1 = 9$, i.e., the total number of unpaired electrons must be eight within the Fe^{III}−Fe^{III} core, Fe^1 in **VI_O** chose to form one d lone pair with only three spins remaining. This complex **VI_O** is thus higher in energy than the corresponding ^{11}A complex **VI_O** in violation of Hund's rule. As expected, the spin density distribution in complex **VII_O** is very similar to that in complex **VI_O**

SCHEME 2: Spin Recoupling Scheme in the Intermediates of the Reaction

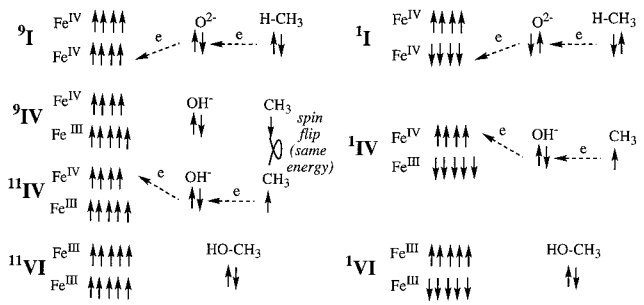

(presented above) for both electronic states, and will not be discussed in detail (see Table 2).

The formal spin-recoupling scheme in the entire reaction pathway is schematically shown in Scheme 2. One can clearly see that, in the C−H activation step, **I** (^{9}A) → **IV** (^{9}A), the electron pair in the C−H bond is broken and an α electron (and a proton) in the bond is transferred to O^{2-} to form an electron pair in the new O−H bond, while an α electron on O^{2-} is transferred to Fe^{IV}. In **IV** (^{9}A), the spin flip on CH_3 to give **IV** (^{11}A) takes place easily. Then the α electron on CH_3 forms a bonding pair with the β electron on the OH^- group, while the α electron on OH^- is transferred to the remaining Fe^{III} to convert it to Fe^{IV} in **VI** (^{11}A). If the two Fe centers are antiferromagnetically coupled to form **I** (^{1}A), essentially the same electron-transfer processes take place for **I** (^{1}A) → **IV** (^{1}A) → **IV** (^{1}A) without spin flip.

Thus, the above-presented data and potential energy profile (PEP) for the O-side pathway of the reaction **I** + CH_4 → **VII** given in Figure 2 show that PEP does not differ much between the ^{9}A and ^{11}A states. In both states, the reaction proceeds from **I** (model of **Q**) via H abstraction on the bridging O^1 center, which is the rate-determining step, and is followed by the formation of methanol between the methyl radical and the bridged O^1H group. When examined in detail, there are some differences in the energetics between the two states, and one can see clear changes in the preferred electronic states of the Fe core as the reaction proceeds. At reactant **I**, the ground state is ^{9}A, lower than ^{11}A by 5.4 kcal/mol, which is reduced to 1.2 kcal/mol at TS1 **III_O**. The ^{9}A ground state of **I** has, qualitatively speaking, an $Fe^{IV}-Fe^{IV}$ core, as suggested experimentally for **Q**, while the ^{11}A state of **I** has an $Fe^{IV}-Fe^{III}$ core and is less stable. Once the system reaches the bound-radical complex **IV_O**, the energy gap between ^{9}A and ^{11}A is reduced to zero. Formally, complex **IV_O** is an $Fe^{IV}-Fe^{III}$ mixed-valence complex for both ^{9}A and ^{11}A states, where the $Fe_2(\mu\text{-}O^2)(\mu\text{-}O^1H)$ core interacts with the methyl radical either ferro- or antiferromagnetically. In the product methanol complex **VI_O**, the ground state becomes ^{11}A, which is 12.1 kcal/mol lower than ^{9}A. Here, the preferred iron core is an $Fe^{III}-Fe^{III}$ and each Fe has five spins, which naturally gives the ^{11}A state when ferromagnetically coupled. In the dissociation limit **VII_O** + HO^1CH_3 the ^{11}A state with two high-spin Fe^{III} centers remains the ground state, and the ^{9}A state with one high-spin and one low-spin Fe^{III} center lies 8.2 kcal/mol higher.

V. Comparison of N-Side and O-Side Pathways

The comparison of the above-presented results on the O-side pathway of the reaction **Q** + CH_4, with those on its N-side pathway, discussed in our previous paper[13] and briefly presented in section III, Table 2, and Figure 2, shows that both pathways proceed via similar intermediates, transition states, and products. The reaction starts by coordination of the CH_4 substrate to a bridging O atom: O^1 located on the same side with the water (glutamate and aspartate ligands, in the real enzyme) molecules in the O-side pathway or the O^2 atom located on the same side with the NH_2 (His ligands in the real enzyme) molecules in the N-side pathway. It then proceeds via the corresponding H-abstraction transition states, **III_O** and **III_N**, and leads to the bound-radical intermediates, **IV_O** and **IV_N**, respectively. This step of the reaction is calculated to be the rate-determining step and proceed through 23.2 and 19.5 kcal/mol barriers for the O-side and N-side pathways, respectively, in the ground ^{9}A states. In other words, the N-side pathway is kinetically more favorable than the O-side one by about 4 kcal/mol. This difference in the activation barriers on the O^1 and O^2 centers most likely relates to the difference in their spin densities; as seen in Table 2, the O^2 center has a more radical character and presumably is more reactive than the O^1 center. The entire reaction **I** + CH_4 → **IV** is calculated to be endothermic by 11.3 and 11.4 kcal/mol, for the O- and N-side pathways, respectively. Subsequently, the methyl radical binds to the bridging OH group via relatively small barriers for both pathways and leads to formation of methanol complexes **VI**. The entire reaction of **I** + CH_4 → **VI** is calculated to be exothermic by 53.9 and 39.8 kcal/mol for the O-side and N-side pathways, respectively.

The spin density analysis (Tables 2 and S2) and the comparison of the PEP of the reaction **I** + CH_4 → **VI** for the ^{9}A and ^{11}A states show that in both cases it starts from the ^{9}A state of **I** with an $Fe^{IV}-Fe^{IV}$ core and reaches the radical complex **IV** with $Fe^{IV}-Fe^{III}$ mixed-valence Fe centers, where the $Fe_2(\mu\text{-}O^2)(\mu\text{-}O^1H)$ core interacts with the methyl radical either ferro- or antiferromagnetically. Then, a spin crossing occurs between the ^{9}A and ^{11}A potential surfaces and the reaction produces the methanol complex **VI** with the ^{11}A ground state and $Fe^{III}-Fe^{III}$ core, where each Fe has five spins.

Thus, the calculations show that both pathways proceed via the bound-radical mechanism. From the computational point of view, the N-side pathway is preferable to the O-side pathway. However, as mentioned above, experiments[2,3] show that the N side of the enzyme is not accessible for the substrate because of steric hindrance and the reaction has to take place only via the O-side mechanism.

VI. Conclusions

From the above-presented results and discussions, one may draw the following conclusions.

(1) The O-side pathway of the reaction of compound **Q** with a molecule of methane proceeds via a bound-radical mechanism. It starts from the bis(μ-oxo) compound **I** (model of **Q**) and goes over the rate-determining transition state **III_O** for H abstraction from methane to form a (μ-O)(μ-OH) intermediate **IV_O** which is weakly complexed with the methyl radical. This intermediate **IV_O** is presumably short-lived and is not likely to be easily detected experimentally, as it is converted via a low barrier at transition state **V_O** for the addition of this methyl radical to the μ-OH ligand to produce the oxo−methanol complex **VI_O**. The latter easily, with about 7−8 kcal/mol energy, eliminates the methanol molecule and produces the Fe(μ-O)Fe, **VII_O**, complex. During the process, the oxidation state of the Fe core changes from $Fe^{IV}-Fe^{IV}$ in **I** to a mixed-valence $Fe^{IV}-Fe^{III}$ in short-lived intermediate **IV_O**, and finally to $Fe^{III}-Fe^{III}$ in **VI_O** and **VII_O**.

I, $L_4Fe^{IV}(\mu\text{-}O)_2Fe^{IV}L_4 + CH_4 \rightarrow$ **III_O**, TS1 for H-atom abstraction (rate-determining) $\rightarrow$ **IV_O**, $L_4Fe^{IV}(\mu\text{-}O^2)(\mu\text{-}O^1H(\cdots CH_3))Fe^{III}L_4$ (bound-radical intermediate) $\rightarrow$ **V_O**, TS2 for CH_3 addition $\rightarrow$ **VI_O**, $L_4Fe^{III}(O^1HCH_3)(\mu\text{-}O^2)Fe^{III}L_4 \rightarrow$ **VII_O**, $L_4Fe^{III}(\mu\text{-}O_2)Fe^{III}L_4 + (O^1HCH_3)$

(2) Comparison of the O-side and N-side pathways of the reaction **Q** + CH_4 shows that both pathways include similar intermediates, transition states, and products, and proceed via the bound-radical mechanism. The rate-determining step of both pathways is the H-atom abstraction from the methane molecule at the transition states **III_O** and **III_N**, respectively, which occurs by 23.2 and 19.5 kcal/mol barriers for the O-side and N-side pathways, respectively, in the ground ^{9}A states of the systems. Thus, the N-side pathway is kinetically more favorable than the O-side one by about 4 kcal/mol. However, it is experimentally unfeasible because of the steric hindrance of the N side of the enzyme.

Acknowledgment. We are grateful to Profs. Dale Edmondson and Vincent Huynh for stimulating discussions. H.B. acknowledges the Visiting Fellowship from the Emerson Center. The present research is in part supported by a grant (CHE-9627775) from the National Science Foundation. Acknowledgment is also made for generous support of computing time at the Bar Ilan University Computer Center, Emerson Center of Emory University, and US National Center for Supercomputing Applications (NCSA).

Supporting Information Available: Table S1, total (in italics, hartrees) and relative (kcal/mol, relative to the reactants) energies of various intermediates and transition states, for spin multiplicities of $2S + 1 = 9$ and 11, for the reaction of MMO with methane on the O side, calculated at the B3LYP level of theory using different basis sets, SBK, SBK(O*), and SBK(CO*), and Table S2, Mulliken atomic spin densities (e) for the various intermediates and transition states of the N-side pathway **I** + methane reaction, calculated at the B3LYP/SBK level. This material is available free of charge via the Internet at http://pubs.acs.org.

References and Notes

(1) (a) Feig, A. L.; Lippard, S. *J. Chem. Rev.* **1994**, *94*, 759. (b) Liu, K. E.; Lippard, S. *J. Adv. Inorg. Chem.* **1995**, *42*, 263.

(2) (a) Waller, B. J.; Lipscomb, J. D. *Chem. Rev.* **1996**, *96*, 2625 and references therein. (b) Shu, L.; Nesheim, J. C.; Kauffmann, K.; Munck, E.; Lipscomb, J. D.; Que, L., Jr. *Science* **1997**, *275*, 515.

(3) Solomon, E.; Brunold, T. C.; Davis, M. I.; Kemsley, J. N.; Lee, S.-K.; Lehnert, N.; Neese, F.; Skulan, A. J.; Yang, Y.-S.; Zhou, J. *Chem. Rev.* **2000**, *100*, 235 and references therein

(4) (a) DeRose, V. J.; Liu, K. E.; Kurtz, D. M., Jr.; Hoffman, B. M.; Lippard, S. J.; *J. Am. Chem. Soc.* **1993**, *115*, 6440. (b) Fox, B. G.; Hendrich, M. P.; Surerus, K. K.; Andersson, K. K.; Froland, W. A.; Lipscomb, J. D. *J. Am. Chem. Soc.* **1993**, *115*, 3688. (c) Thomann, H.; Bernardo, M.; McCormick, J. M.; Pulver, S.; Andersson, K. K.; Lipscomb, J. D.; Solomon, E. I. *J. Am. Chem. Soc.* **1993**, *115*, 8881.

(5) (a) Rosenzweig, A. C.; Fredrick, C. A.; Lippard, S. J.; Nordlung, P. *Nature* **1993**, *366*, 537. (b) Rosenzweig, A. C.; Nordling, P.; Takahara, P. M.; Fredrick, C. A.; Lippard, S. J. *Chem. Biol.* **1995**, *2*, 409.

(6) Elango, N.; Radhakrishman, R.; Froland, W. A.; Waller, B. J.; Earhart, C. A.; Lipscomb, J. D.; Ohlendorf, D. H. *Protein Sci.* **1997**, *6*, 556. (b) Nesheim, J. C.; Lipscomb, J. D. *Biochemistry* **1996**, *35*, 10240 and references therein.

(7) (a) Andersson, M. E.; Högbom, M.; Rinaldo-Matthis, A.; Andersson, K. K.; Sjöberg, B.-M.; Nordlund, P. *J. Am. Chem. Soc.* **1999**, *121*, 2346−2352. (b) Herold, S.; Lippard, S. J. *J. Am. Chem. Soc.* **1997**, *119*, 145−156. (c) LeCloux, D. D.; Barrios, A. M.; Mizoguchi, T. J.; Lippard, S. J. *J. Am. Chem. Soc.* **1998**, *120*, 9001−9014. (d) Zhang, X.-X.; Fuhrmann, P.; Lippard, S. J. *J. Am. Chem. Soc.* **1998**, *120*, 10260−10261. (e) Lee, D.; Lippard, S. J. *J. Am. Chem. Soc.* **1998**, *120*, 12153−12154. (f) Voegtli, W. C.; Khidekel, N.; Baldwin, J.; Ley, B. A.; Bollinger, J. M., Jr.; Rosenzwerg, A. C. *J. Am. Chem. Soc.* **2000**, *122*, 3255.

(8) Torrent, M.; Musaev, D. G.; Morokuma, K. *J. Phys. Chem. B* **2001**, *105*, 322.

(9) (a) Liu, K. E.; Wang, D.; Huynh, B. H.; Edmondson, D. E.; Salifoglou, A.; Lippard, S. J. *J. Am. Chem. Soc.* **1995**, *116*, 7465. (b) Liu, K. E.; Valentine, A. M.; Wang, D.; Huynh, B. H.; Edmondson, D. E.; Salifoglou, A.; Lippard, S. J. *J. Am. Chem. Soc.* **1995**, *117*, 10174. (c) Liu, K. E.; Valentine, A. M.; Qiu, D.; Edmondson, D. E.; Appelman, E. H.; Spiro, T. G.; Lippard, S. J. *J. Am. Chem. Soc.* **1995**, *117*, 4997.

(10) Wilkinson, E. C.; Dong, Y.; Zang, Y.; Fujii, H.; Fraczkiewicz, R.; Fraczkiewicz, G.; Czernuszewicz, R. S.; Qui, L., Jr. *J. Am. Chem. Soc.* **1998**, *120*, 955.

(11) Lee, S. K.; Nesheim, J. C.; Lipscomb, J. D. *J. Biol. Chem.* **1993**, *268*, 21569.

(12) Torrent, M.; Mogi, K.; Basch, H.; Musaev, D. G.; Morokuma, K. *J. Phys. Chem. B* **2001**, in press.

(13) Basch, H.; Mogi, K.; Musaev, D. G.; Morokuma, K. *J. Am. Chem. Soc.* **1999**, *121*, 7249.

(14) Valentine A. M.; Stahl, S. S.; Lippard, S. J. *J. Am. Chem. Soc.* **1999**, *121*, 3876.

(15) (a) Yoshizawa, K.; Shiota, Y.; Yamabe, T. *Chem. Eur. J.* **1997**, *3*, 1160. (b) Yoshizawa, K.; Shiota, Y.; Yamabe, T. *J. Am. Chem. Soc.* **1998**, *120*, 564. (c) Yoshizawa, K.; Shiota, Y.; Yamabe, T. *Organometallics* **1998**, *17*, 2825.

(16) (a) Siegbahn, P. E. M.; Crabtree, R. H. *J. Am. Chem. Soc.* **1997**, *119*, 3103. (b) Yoshizawa, K.; Ohta, T.; Yamabe, T. *Bull. Chem. Soc. Jpn.* **1998**, *71*, 80862. (c) Siegbahn, P. E. M.; Crabtree, R. H.; Nordlund, P. *J. Biol. Inorg. Chem.* **1998,** *3*, 314. (d) Siegbahn, P. E. M. *Inorg. Chem.* **1999**, *38*, 2880.

(17) Dunietz, B. D.; Beachy M. D.; Cao, Y.; Whittington, D. A.; Lippard, S. J.; Friesner, R.A. *J. Am. Chem. Soc.* **2000**, *122*, 2828.

(18) (a) Becke, A. D. *Phys. Rev. A* **1988**, *38*, 3098. (b) Becke, A. D. *J. Am. Chem. Soc.* **1993**, *98*, 1372. (c) Becke, A. D. *J. Chem. Phys.* **1993**, *98*, 5648. (d) Lee, C.; Yang, W.; Parr, R. G. *Phys. Rev. B* **1988**, *37*, 785.

(19) (a) Stevens, W. J.; Basch, H.; Krauss, M. *J. Chem. Phys.* **1984**, *81*, 6026. (b) Stevens, W. J.; Krauss, M.; Basch, H.; Jasien, P. G. *Can. J. Chem.* **1992**, *70*, 612.

(20) (a) Musaev, D. G.; Morokuma, K. *J. Phys. Chem.* **1996**, *100*, 6509. (b) Erikson, L. A.; Pettersson, L. G. M.; Siegbahn, P. E. M.; Wahlgren, U. *J. Chem. Phys.* **1995**, *102*, 872. (c) Ricca, A.; Bauschlicher, C. W., Jr. *J. Phys. Chem.* **1994**, *98*, 12899. (d) Heinemann, C.; Hertwig, R. H.; Wesendrup, R.; Koch, W.; Schwarz, H. *J. Am. Chem. Soc.* **1995**, *117*, 495. (e) Hertwig, R. H.; Hrusak, J.; Schroder, D.; Koch, W.; Schwarz, H. *Chem. Phys. Lett.* **1995,** *236*, 194. (f) Schroder, D.; Hrusak, J.; Hertwig, R. H.; Koch, W.; Schwerdtfeger, P.; Schwarz, H. *Organometallics* **1995**, *14*, 312. (g) Fiedler, A.; Schroder, D.; Shaik, S.; Schwarz, H. *J. Am. Chem. Soc.* **1994**, *116*, 10734. (h) Fan, L.; Ziegler, T. *J. Chem. Phys.* **1991**, *95*, 7401. (i) Berces, A.; Ziegler, T.; Fan, L. *J. Phys. Chem.* **1994**, *98*, 1584. (j) Lyne, P. D.; Mingos, D. M. P.; Ziegler, T.; Downs, A. J. *Inorg. Chem.* **1993**, *32*, 4785.(k) Li, J.; Schreckenbach, G.; Ziegler, T. *J. Am. Chem. Soc.* **1995**, *117*, 486.

(21) Gaussian 94, Revision D.3: Frisch, M. J.; Trucks, G. W.; Schlegel, H. B.; Gill, P. M. W.; Johnson, B. G.; Robb, M. A.; Cheeseman, J. R.; Keith, T. A.; Petersson, J. A.; Montgomery, J. A.; Raghavachari, K.; Al-Laham, M. A.; Zakrzewski, V. G.; Ortiz, J. V.; Foresman, J. B.; Cioslowski, J.; Stefanov, B. B.; Nanayakkara, A.; Challacombe, M.; Peng, C. Y.; Ayala, P. Y.; Chen, W.; Wong, M. W.; Andres, J. L.; Replogle, E. S.; Gomperts, R.; Martin, R. L.; Fox, D. J.; Binkley, J. S.; DeFrees, D. J.; Baker, J.; Stewart, J. J. P.; Head-Gordon, M.; Gonzales, C.; Pople, J. A., Gaussian Inc., Pittsburgh, PA, 1995.

(22) Valentine, A. M.; Wikinson, B.; Liu, K. E.; Komar-Panicucci, S.; Priestley, N. D.; Williams, P. G.; Morimoto, H.; Floss, H. G.; Lippard, S. J. *J. Am. Chem. Soc.* **1997**, *119*, 1818.